Feasibility of terahertz reflectometry for discrimination of human early gastric cancers

Young Bin Ji,[1,11] Chan Hyuk Park,[2,11] Hyunki Kim,[3] Sang-Hoon Kim,[4] Gyu Min Lee,[5] Sam Kyu Noh,[6] Tae-In Jeon,[7] Joo-Hiuk Son,[8] Yong-Min Huh,[4,9] Seungjoo Haam,[1,10] Seung Jae Oh,[4,12] Sang Kil Lee,[2,13] and Jin-Suck Suh[4,9,*]

[1]Yonsei Institute of Convergence Technology, Yonsei University, Seoul 120-752, South Korea
[2]Division of Gastroenterology, Department of Internal Medicine, Severance Hospital, Institute of Gastroenterology, Yonsei University College of Medicine, Seoul, 120-752, South Korea
[3]Department of Pathology, Yonsei University College of Medicine, Seoul 120-752, South Korea
[4]YUMC-KRIBB Medical Convergence Research Institute, Yonsei University College of Medicine, Seoul 120-752, South Korea
[5]Graduate Program for Nanomedical Science, Yonsei University, Seoul 120-749, South Korea
[6]Nano Materials Evaluation Center, Korea Research Institute of Standards and Science, Daejeon 305-340, South Korea
[7]Division of Electrical and Electronics Engineering, Korea Maritime University, Busan 606-791, South Korea
[8]Department of Physics, University of Seoul, Seoul 130-743, South Korea
[9]Department of Radiology, Severance Biomedical Science Institute, Yonsei University College of Medicine, Seoul 120-752, South Korea
[10]Department of Chemical and Biomolecular Engineering, Yonsei University, Seoul 120-749, South Korea
[11]These authors contributed equally to this work.
[12]issac@yuhs.ac
[13]sklee@yuhs.ac
*jss@yuhs.ac

Abstract: We have investigated the feasibility of THz time-domain reflectometry for the discrimination of human early gastric cancer (EGC) from the normal gastric region. Eight fresh EGC tissues, which were resected by endoscopic submucosal dissection, were studied. Of them, six lesions were well discriminated on THz images and the regions well correlated with tumor regions on pathologically mapped images. Four THz parameters could be suggested for quantitative discrimination of EGCs.

References and links

1. R. M. Woodward, V. P. Wallace, R. J. Pye, B. E. Cole, D. D. Arnone, E. H. Linfield, and M. Pepper, "Terahertz pulse imaging of ex vivo basal cell carcinoma," J. Invest. Dermatol. **120**(1), 72–78 (2003).
2. V. P. Wallace, A. J. Fitzgerald, S. Shankar, N. Flanagan, R. Pye, J. Cluff, and D. D. Arnone, "Terahertz pulsed imaging of basal cell carcinoma ex vivo and in vivo," Br. J. Dermatol. **151**(2), 424–432 (2004).
3. S. J. Oh, J. Kang, I. Maeng, J.-S. Suh, Y.-M. Huh, S. Haam, and J.-H. Son, "Nanoparticle-enabled terahertz imaging for cancer diagnosis," Opt. Express **17**(5), 3469–3475 (2009).
4. A. J. Fitzgerald, V. P. Wallace, M. Jimenez-Linan, L. Bobrow, R. J. Pye, A. D. Purushotham, and D. D. Arnone, "Terahertz pulsed imaging of human breast tumors," Radiology **239**(2), 533–540 (2006).
5. P. C. Ashworth, E. Pickwell-MacPherson, E. Provenzano, S. E. Pinder, A. D. Purushotham, M. Pepper, and V. P. Wallace, "Terahertz pulsed spectroscopy of freshly excised human breast cancer," Opt. Express **17**(15), 12444–12454 (2009).
6. S. J. Oh, S.-H. Kim, Y. B. Ji, K. Jeong, Y. Park, J. Yang, D. W. Park, S. K. Noh, S. G. Kang, Y. M. Huh, J. H. Son, and J. S. Suh, "Study of freshly excised brain tissues using terahertz imaging," Biomed. Opt. Express **5**(8), 2837–2842 (2014).
7. Y. C. Sim, J. Y. Park, K.-M. Ahn, C. Park, and J.-H. Son, "Terahertz imaging of excised oral cancer at frozen temperature," Biomed. Opt. Express **4**(8), 1413–1421 (2013).
8. Y. B. Ji, E. S. Lee, S.-H. Kim, J.-H. Son, and T.-I. Jeon, "A miniaturized fiber-coupled terahertz endoscope system," Opt. Express **17**(19), 17082–17087 (2009).

9.   S. Y. Huang, Y. X. J. Wang, D. K. W. Yeung, A. T. Ahuja, Y.-T. Zhang, and E. Pickwell-Macpherson, "Tissue characterization using terahertz pulsed imaging in reflection geometry," Phys. Med. Biol. **54**(1), 149–160 (2009).
10. Y. B. Ji, S.-H. Kim, K. Jeong, Y. Choi, J.-H. Son, D. W. Park, S. K. Noh, T.-I. Jeon, Y.-M. Huh, S. Haam, S. K. Lee, S. J. Oh, and J.-S. Suh, "Terahertz spectroscopic imaging and properties of gastrointestinal tract in a rat model," Biomed. Opt. Express **5**(12), 4162–4170 (2014).
11. C. B. Reid, A. Fitzgerald, G. Reese, R. Goldin, P. Tekkis, P. S. O'Kelly, E. Pickwell-MacPherson, A. P. Gibson, and V. P. Wallace, "Terahertz pulsed imaging of freshly excised human colonic tissues," Phys. Med. Biol. **56**(14), 4333–4353 (2011).
12. L. H. Eadie, C. B. Reid, A. J. Fitzgerald, and V. P. Wallace, "Optimizing multi-dimensional terahertz imaging analysis for colon cancer diagnosis," Expert Syst. Appl. **40**(6), 2043–2050 (2013).
13. A. Jemal, F. Bray, M. M. Center, J. Ferlay, E. Ward, and D. Forman, "Global cancer statistics," CA Cancer J. Clin. **61**(2), 69–90 (2011).
14. K.-W. Jung, Y.-J. Won, H.-J. Kong, C.-M. Oh, D. H. Lee, and J. S. Lee, "Cancer Statistics in Korea: Incidence, Mortality, Survival, and Prevalence in 2011," Cancer Res. Treat. **46**(2), 109–123 (2014).
15. D. Hou, X. Li, J. Cai, Y. Ma, X. Kang, P. Huang, and G. Zhang, "Terahertz spectroscopic investigation of human gastric normal and tumor tissues," Phys. Med. Biol. **59**(18), 5423–5440 (2014).
16. C. H. Park, B. Kim, H. Chung, H. Lee, J. C. Park, S. K. Shin, S. K. Lee, and Y. C. Lee, "Endoscopic Quality indicators for esophagogastroduodenoscopy in gastric cancer screening," Dig. Dis. Sci. Epub ahead of print (2014).
17. M. S. Park, J. Y. Yoon, H. S. Chung, H. Lee, J.C. Park, S. K. Shin, S. K. Lee, and Y.C. Lee, "Clinicopathologic characteristics of interval gastric cancer in Korea." Gut Liver Epub ahead of print (2014).
18. Y. S. Cho, I.-K. Chung, J. H. Kim, Y. Jung, T. H. Lee, S.-H. Park, and S.-J. Kim, "Risk factors of developing interval early gastric cancer after negative endoscopy," Dig. Dis. Sci. Epub ahead of print (2014).
19. K. J. Kwon, K. N. Shim, E. M. Song, J. Y. Choi, S. E. Kim, H. K. Jung, and S. A. Jung, "Clinicopathological characteristics and prognosis of signet ring cell carcinoma of the stomach," Gastric Cancer **17**(1), 43–53 (2014).
20. B. H. Min, K. J. Kang, J. H. Lee, E. R. Kim, Y. W. Min, P. L. Rhee, J. J. Kim, J. C. Rhee, and K. M. Kim, "Endoscopic resection for undifferentiated early gastric cancer: focusing on histologic discrepancies between forceps biopsy-based and endoscopic resection specimen-based diagnosis," Dig. Dis. Sci. **59**(10), 2536–2543 (2014).
21. P. Doradla, K. Alavi, C. Joseph, and R. Giles, "Single-channel prototype terahertz endoscopic system," J. Biomed. Opt. **19**(8), 080501 (2014).
22. S. M. Kim, F. Hatami, J. S. Harris, A. W. Kurian, J. Ford, D. King, G. Scalari, M. Giovannini, N. Hoyler, J. Faist, and G. Harris, "Biomedical terahertz imagin with a quantum cascade laser," Appl. Phys. Lett. **88**(15), 153903 (2006).
23. Y. L. Lim, T. Taimre, K. Bertling, P. Dean, A. Indjin, A. Valavanis, S. P. Khanna, M. Lachab, H. Schaider, T. W. Prow, H. Peter Soyer, S. J. Wilson, E. H. Linfield, A. Giles Davies, and A. D. Rakić, "High-contrast coherent terahertz imaging of porcine tissue via swept-frequency feedback interferometry," Biomed. Opt. Express **5**(11), 3981–3989 (2014).

1. Introduction

Terahertz (THz) reflectometry has been applied to many biomedical researches, especially cancer diagnosis [1–7]. Diagnoses of skin and breast cancer were preceded using THz reflectometry because it was relatively easy to obtain the specimens and conduct in vivo experiments [1–5]. In recent years, THz studies have been extended to new tissue lesions such as brain and tongue cancer [6,7].

Meanwhile, as the potential production of miniaturized THz endoscopes has increased [8], interest in applications for digestive organ cancers, which had received poor attention due to the limitations of the THz device and system, has rapidly grown. Accordingly, during the past few years, the basic tissue characteristics of each digestive organ in the THz regime have been investigated [9,10], and THz reflectometry was proven as a tool for the diagnosis of human colorectal cancer by using several THz parameters and statistical analysis [11,12]. With regard to gastric cancer, which has high incidence rates in Eastern Asia [13,14], few investigation using THz reflectometry have been carried out until last year [15]. The possibility of diagnosing gastric cancer using THz waves in dehydrated paraffin-embedded tissues was suggested.

Although advanced gastric cancers have shown poor prognosis [13], a high cure rate approaching 90% can be achieved by surgery in patients with early staged gastric cancers [15]. Recent technical advances show that early gastric cancer (EGC) fulfilled indication of endoscopic resection can be treated successfully by endoscopic resection including

endoscopic submucosal dissection (ESD) rather than surgery which involves pain and a long recovery time. In addition, the patient's quality of life can be improved by treatment with endoscopic resection compared with open surgery, because endoscopic resection is a method to preserve the whole stomach after treatment. Therefore, it is ultimately important to find gastric cancer as early as possible to improve patient survival and quality of life after treatment.

When EGC is viewed at an early developmental stage, abnormalities by white light endoscopy tend to be subtle. It is possible to miss some cases of EGC, as white light endoscopy is an operator-dependent procedure [16–18]. If THz reflectometry help detect an EGC lesion and delineate its margins quantitatively, it would assist endoscopists in determining the lesion size and completely resecting the target lesion with appropriate and safe margins.

In this study, we aimed to evaluate the feasibility of THz time-domain reflectometry for the discrimination of EGC from normal tissues using fresh excised tissue specimens obtained from patients who had undergone ESD. THz reflection images for the fresh tissues were taken by a conventional, reflection mode THz time-domain imaging system with photoconductive antennas. THz reflection images were compared with visible gross images and pathologically mapped images. In addition, several parameters extracted from the THz reflection signals were analyzed to quantitatively discriminate EGC from adjacent normal regions.

2. Specimen preparation and experimental details

2.1 Specimen preparation

The study protocol was approved by the Institutional Review Board and Hospital Research Ethics Committee of Severance Hospital. Written informed consent was obtained from all patients. Nine patients with EGC that was treated with ESD were recruited for this study. Of the nine patients, one with an incompletely resected lesion by ESD was excluded because the circumferential margins of the lesion were not fully included in the specimen. As a result, eight patients with completely resected EGC by ESD were enrolled in the study.

ESD was performed in accordance with the typical procedure sequence consisting of marking, mucosal incision, and submucosal dissection with simultaneous hemostasis. To prevent deep muscle injury during the procedure, a saline solution containing epinephrine (0.01 mg/mL) was injected into the submucosal layer circumferentially around the lesion using a 21-gauge needle before initiating the mucosal incision (Fig. 1(a)). Immediately after the end of ESD, the specimens were delivered for taking THz reflection images.

Table 1 shows baseline patient and lesion characteristics. Of eight lesions, seven were well- to moderate differentiated adenocarcinomas, and the remaining one was a signet ring cell carcinoma. All lesions were confined to the mucosa. The median lesion size was 7 mm (range, 4–20 mm).

Table 1. Baseline patient and lesion characteristics.

Case	Gender	Age	Location	Histology	Depth of invasion	Cancer size (mm)
1	Female	63	Antrum	AWD	Mucosa	20
2	Female	58	Antrum	AMD	Mucosa	8
3	Male	61	Antrum	AWD	Mucosa	6
4	Female	53	Antrum	AWD	Mucosa	10
5	Male	62	Antrum	SRC	Mucosa	6
6	Female	44	Antrum	AWD	Mucosa	4
7	Female	63	Upper body	AWD	Mucosa	15
8	Male	68	Antrum	AMD	Mucosa	5

AWD, adenocarcinoma well-differentiated; AMD, adenocarcinoma moderate differentiated; SRC, signet ring cell carcinoma.
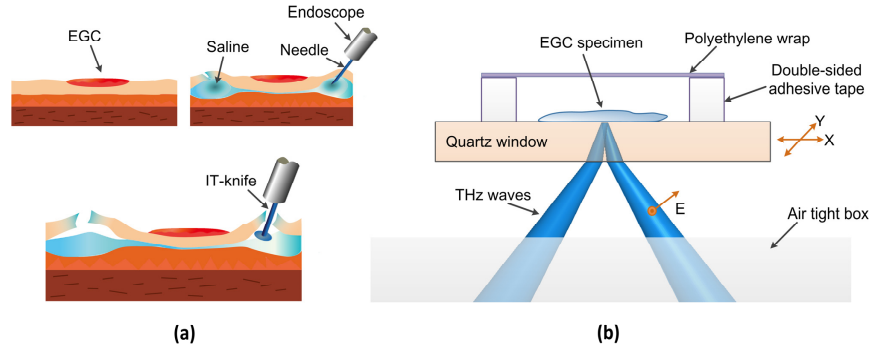
2.2 Experimental setup

Fig. 1. Schematic diagrams. (a) Specimen preparation by ESD. (b) THz time-domain reflectometry experimental setup.

A conventional THz time-domain imaging system with photoconductive antennas and a fast optical delay line was utilized in our experiments in reflection mode. Because the resected specimens are used for formal histopathological examination after THz measurement, no additional handling processes were applied to the specimen to prevent unwanted contamination except for carefully removing a little blood on the surface of the specimens by cotton swabs. For the same reason, we reduced the acquisition time of the THz measurements. Thus, the THz images were obtained with a raster scanning system using a two-dimensional (2D) movable sample stage with sparse resolution. The total acquisition time per THz image was approximately 8 min for a 50 × 47.5-mm area with a 500-μm scanning resolution. The total time of the THz experiment from receiving the specimens to putting the specimens into a fixation bottle was less than 30 min. The schematic diagram of the measurement system is shown in Fig. 1(b), and a more detailed description is presented in our previous article [10].

2.3 Image and parameter extraction

Note that the aim of this study is not a diagnosis of EGC but a discrimination of EGC under endoscopic conditions. Accordingly, we considered simple parameters among the various THz parameters to acquire the images and quantifications. All THz images were made of peak-to-peak (PP) values extracted from reflection signals on the quartz/specimen interface and normalized by the PP value on the quartz/water interface. To demonstrate that the THz technique would quantitatively discriminate EGC from normal regions, four parameters were utilized. Two were PP values at the region of interest (ROI) on the THz images normalized to each of two reference PP values (water and air), whereas the others were amplitude ratios of spectra at ROIs normalized to each of two reference spectra (water and air). The ROIs for each EGC and normal region were selected from five points on each THz image, which included pathologically confirmed regions (Fig. 2(b)). Table 2 shows a summary of the THz parameters used. PPV(t) is a PP value of the time-domain reflection signal, and E(ω) is the spectrum amplitude of the reflection signal.

Table 2. Summary of THz parameters for discrimination of EGC and normal regions.

Parameter	Water reference	Air reference
1 and 2	$PPV_{specimen}(t)/PPV_{water}(t)$	$PPV_{specimen}(t)/PPV_{air}(t)$
3 and 4	$E_{specimen}(\omega)/E_{water}(\omega)$	$E_{specimen}(\omega)/E_{air}(\omega)$

3. Results and discussion

Among the eight lesions enrolled in the study, seven were well discriminated on THz images. Representative images included gross tumor images, THz images and pathologically mapped

images of three different lesions (cases 1, 2, and 3) are shown in Fig. 2. The red regions of Fig. 2(c) indicate the lesions of pathologically confirmed EGC. The cancers are well discriminated even in visible gross images as shown in Fig. 2(a), which reflects that endoscopists could find EGC by white light endoscopy only. However, endoscopic examination for gastric cancer screening is an operator-dependent procedure [16]. Such a nature of endoscopic examination may be related with missing gastric cancer [17,18]. Thus, we suggest THz imaging and technique to reduce the chance of missing cases of EGC.
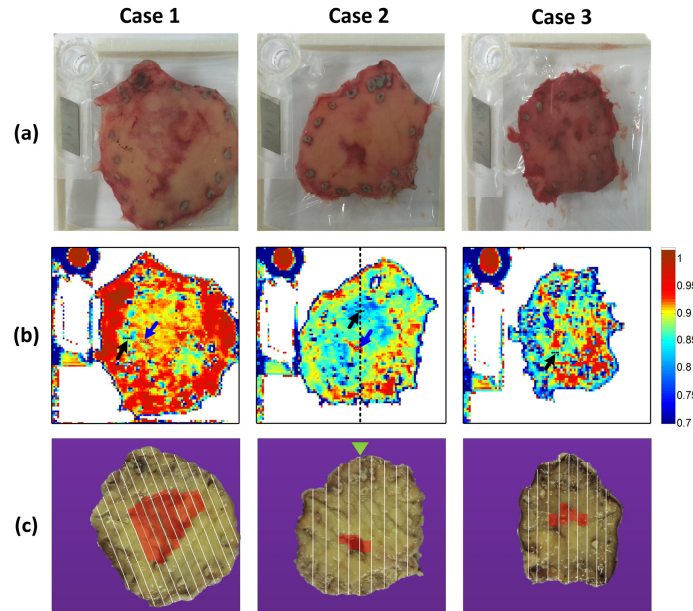

Fig. 2. Comparison of images in three different EGC cases. (a) Visible gross images. (b) PP THz images. The selected ROIs for THz parameters of the EGC and normal regions are indicated by blue arrows and black arrows, respectively. (c) Pathologically mapped images. White lines represent the 2-mm slices obtained for pathologic examination. Red region, pathologically proven gastric cancer.

The acquired THz images are shown in Fig. 2(b). Although the THz reflection intensity from the normal regions is generally low because they have low refractive indices and low absorption coefficients compared with tumors in the THz regime [1, 2, 4–6, 11], in all THz images, high intensity signals were noted around the circumference of the ESD specimens which were pathologically confirmed as normal regions. This aspect caused confusion during the discrimination of EGC from normal regions on THz images during the initial analysis stage. It is assumed to be due to the effect of saline, which was injected around the lesion during the ESD.

Foundation of our assumption that the high intensity signal at the border of the specimen is attributed to saline effect came from THz measurements of EGC. Figure 3(a) shows a case 1 THz image where five data points of water and normal tissue are marked in. And Fig. 3(b) shows time-domain THz signals at marked points in Fig. 3(a). Regardless of selecting histologically normal tissue points, THz reflection signals from normal 1 and 3 appear much larger than those from normal 2 and 4. Furthermore, the amplitude of reflection signals from normal 1 and 3 are very similar those from water as shown in Fig. 3(b). Therefore, we assumed that the high intensity signal could be generated by absorbed saline at the border of the specimen where we injected saline. The endoscopic submucosal dissection (ESD) procedure sequence consists of 3 steps including 1) marking, 2) mucosal incision, and then 3) submucosal dissection. Saline injection is needed in 2) mucosal incision, and 3) submucosal

dissection for preventing the perforation. Although these two steps need saline injection, the amount of saline is much larger for 2) mucosal incision compared to 3) submucosal dissection (Fig. 1(a)). In the steps of 2) mucosal incision, saline is likely to go into mucosal layer as well as submucosal layer because the needle reached submucosa via mucosal layer. In the steps of 3) submucosal dissection, needle reached submucosa directly without intervening tissues. We consider all these two factors can cause exacerbation of saline effect on periphery.
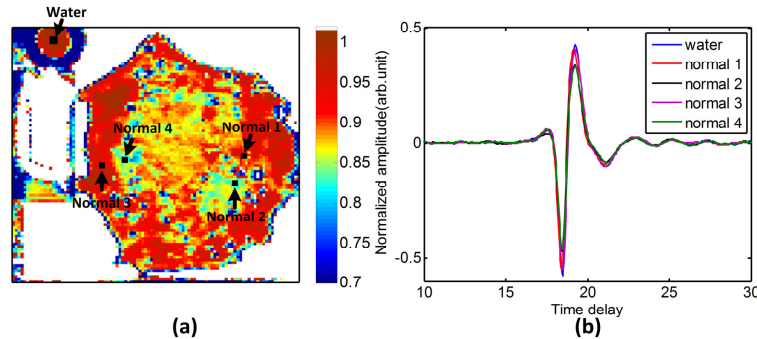

(a)   **(b)**

Fig. 3. The saline effect on THz image. (a) THz image of case 2 where data points of water and normal tissue are marked in. (b) Time-domain THz signals at marked points in Fig. 3(a). Despite all selected normal tissue points are histologically same, THz reflection signals from normal 1 and 3 much larger than those from normal 2 and 4 due to the injected saline.

The THz image of case 2 supports this assumption as reasonable. Low-intensity normal regions are observed around the center of the specimen except for the tumor region in that image. Before the injection of saline, the reflection signals from the normal region would be lower than those from the tumor region. In addition, high intensity regions in the center of the specimen were also discriminated from the surrounding low-intensity regions.

Although seven of the eight lesions were discriminated by THz imaging, a distinct boundary of the remaining lesion was unclear on the THz image, because the effects of the saline injection during the ESD procedure appeared too close to the lesion (case 4, image not shown). In this case, high intensity signals around the margin of the ESD specimen prevented the delineation of EGC. However, this finding may not discount the feasibility of in vivo THz imaging for discrimination of gastric cancer. Of seven lesions discriminated by THz imaging, six well-to moderate differentiated adenocarcinomas were well correlated with pathologically mapped images. The one lesion with poor correlation between the THz and pathologically mapped images was a signet ring cell carcinoma (case 5, image not shown). Generally, the biological behavior of signet ring cell carcinoma is considered to be different from other cell types, including gastric adenocarcinoma [19]. In addition, large size discrepancies are frequently observed in signet ring cell carcinoma between gross findings and pathologic examinations [20]. THz imaging may play a limited role in the discrimination of signet ring cell carcinoma.

To confirm a congruence between the pathology and the THz images, and to assume the contrast mechanisms, we compared and analyzed an hematoxylin and eosin (H&E)-stained photomicrograph with the normalized THz PP values for case 2 (Fig. 4). Figure 4(a) shows parameter 1 profiles along a black dashed line on the THz image shown in Fig. 2(b). The black dashed line corresponds with the axis of the histological section as indicated by a yellow-green triangle in Fig. 2(c). The region with a high amplitude ratio displayed in red was well correlated with the tumor region. The inset on Fig. 4(a) is the image of case 2 (Fig. 2(c)) which was cropped and rotated for easy comparison. Figure 4(b) shows a cross-sectional microscopic image of the axis of the yellow-green mark in Fig. 2(c) at low magnification (× 12), including both tumor and normal regions. Figure 4(c) and 4(d) are enlarged images of tumor and normal regions, respectively, at high magnification (× 100) of the regions marked

by dashed black rectangles in Fig. 4(b). In contrast to the normal region, microvascular proliferation and increased cellular density were identified in the tumor region. The contrast mechanisms for discriminating tumors using THz reflectometry would involve the complex physiological changes from increases in water content, cell density, vascularity, etc [4, 15].
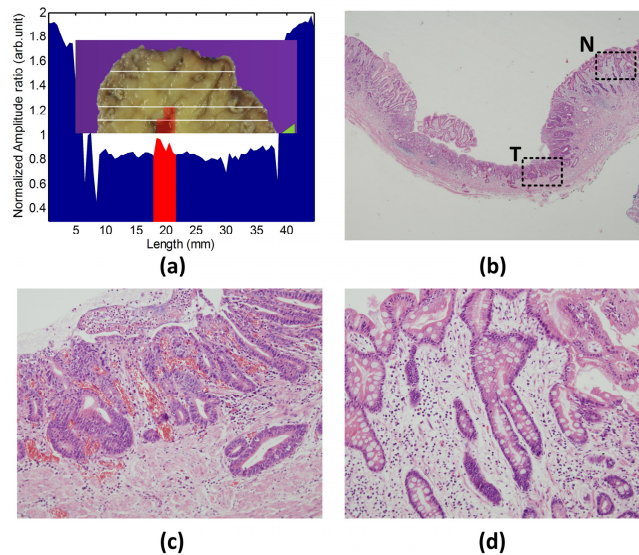

Fig. 4. (a) THz PP value profiles normalized to the water reference along the black dashed line on the THz image in Fig. 2(b). The inset is from the case 2 image in Fig. 2(c), which was cropped and rotated for easy comparison. (b) A section of the H&E-stained microphotograph at low magnification (× 12) of the axis indicated by a yellow-green triangle in Fig. 2(c). (c), (d) Amplified images (× 100) of tumor and normal mucosa, respectively, marked by dashed rectangles in (b) where T and N indicate tumor and normal mucosa.

The normalized and average PP values (parameters 1 and 2) from the ROIs were evaluated for lesions except one whose boundary was unclear because of saline effects around the lesion (case 4) and one signet ring cell carcinoma (case 5) (Fig. 5). The error bars arise from different points within the ROIs (note these small error bars may come from being too confined in the selection of the ROIs for each case due to the saline effect). Both parameters show that the THz reflection intensities from the quartz/EGG interface were higher than those from the quartz/normal mucosa interface in all six cases. Both parameters show that THz reflectometry is able to discriminate EGC from normal regions quantitatively. Parameter 1 has an advantage in that it provides a higher contrast than parameter 2, but it would vary with the temperature of the water (in our study, room temperature was kept always constant). On the other hand, parameter 2 provides a consistent, low contrast compared with parameter 1. Because the water and air reference signals can be easily obtained in practical situations, these two parameters would be valuable for the discrimination of EGC under endoscopic conditions.
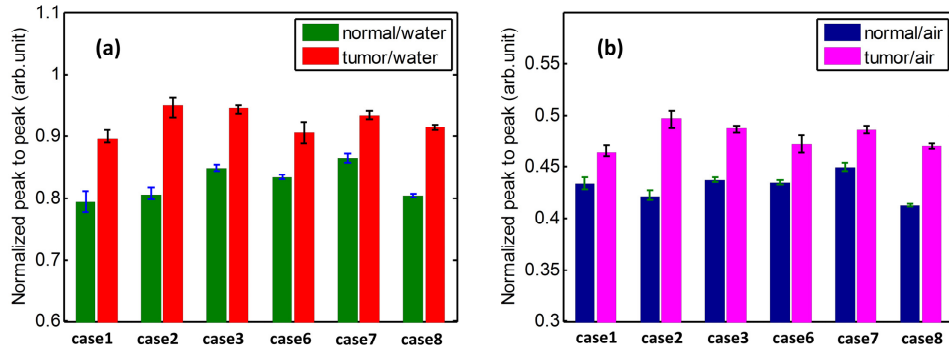
Fig. 5. Average PP values with error bars taken from the ROIs of six cases. (a) The PP values normalized to the PP value of the water reference. (b) PP values normalized to the PP value of the air reference. EGCs are well discriminated from normal mucosa by these two parameters.
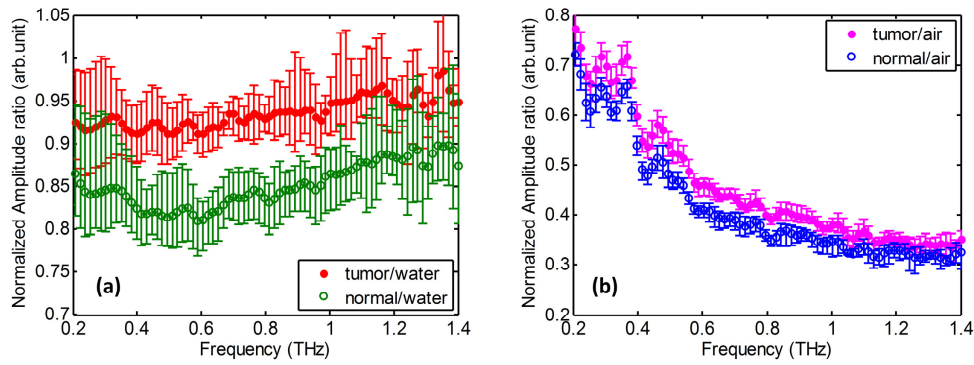

Fig. 6. Average THz spectra with error bars taken from the ROIs of six cases. (a) The spectra normalized to the spectrum of the water reference. (b) Spectra normalized to the spectrum of the air reference. Cases 4 and 5 were excluded for these analyses. EGCs are well discriminated in the specific THz regime (0.4~1THz).

Figure 6 shows normalized and average THz spectra of EGC and normal mucosa of six cases (parameters 3 and 4). Each of the six spectra obtained by fast Fourier transform performed on the averaged THz time-domain signals of the previously selected ROIs. All six spectra were averaged again. The error bars show variations in the normalized amplitude ratios at each frequency derived from variations of the six patients. Figure 6 shows that discrimination of EGC from normal mucosa is possible in the specific THz regime. In our results, the normalized amplitude ratios of EGC are higher than those of normal mucosa in the range from 0.4 THz to 1 THz; furthermore, even the error bars do not overlap in that range. On the other hand, although the averaged amplitude ratios can be distinguished in the range of 0.2~0.4 THz and beyond 1 THz, the error bars overlap in these ranges. This spectral feature may be partially related to the absorption coefficient of normal mucosa. It was previously reported that dehydrated normal tissue may have a higher absorption coefficient than dehydrated tumor tissue in specific THz regime [15]. Using parameters 3 and 4, we are able to distinguish EGC using THz reflectometry in the specific frequency from 0.4 THz to 1 THz.

4. Summary and conclusions

We have investigated the feasibility of THz reflectometry for the discrimination of EGC from adjacent normal gastric regions. Eight fresh EGC tissues that were resected by ESD were studied. The THz reflection intensities from EGCs were higher than from normal mucosa, thus the EGCs were well discriminated in the normalized PP THz images. Six of eight lesions

were well discriminated on THz images and the regions well correlated with tumor regions on pathologically mapped images. The result of signet ring cell carcinoma, which was not correlated well between the THz and pathologically mapped images implied that THz imaging may play a limited role in the discrimination of signet ring cell carcinoma. In addition, four THz parameters were suggested for the quantitative discrimination of well- to moderate differentiated adenocarcinomas.

We expect that future work that involves in vivo feasibility tests for preclinical and clinical uses will be conducted. However, these studies should include the development of a reliable miniaturized THz endoscope. Attempts to develop a practical THz endoscope have been continued [21], in addition, various novel THz imaging techniques such as THz-QCL imaging have been applied to biomedical research [22,23]. We expect this feasibility study to help develop a THz endoscope for the discrimination of EGC and other digestive organ cancers.

Acknowledgments